

# Robotic Drilling of Aluminum Alloy Performance and Hole Quality

Fouad Messaoudi<sup>1</sup>, Abdelhakim Djebara<sup>1,2\*</sup>, Mohamed Djennane<sup>1</sup>

<sup>1</sup> Laboratory of Mechanics and Advanced Energy Systems, Mechanical Engineering Department, National Polytechnic School of Constantine, P. O. B. 75, A, Constantine 25000, Algeria

<sup>2</sup> Laboratory of Structural Mechanics and Materials, Department of Mechanical Engineering, University of Batna 2, 53 Constantine Road, Fesdis 05078, Batna, Algeria

\* Corresponding author, e-mail: [ab.djebara@univ-batna2.dz](mailto:ab.djebara@univ-batna2.dz)

Received: 09 June 2023, Accepted: 19 July 2023, Published online: 27 July 2023

## Abstract

This paper presents an experimental approach to evaluate the ability of a six-axis industrial robot to drill aluminum alloy parts. A strategy based on statistical tests has been studied to quantify and predict the relative contribution of cutting parameters on cutting force and shape errors during drilling. This technique is based on the identification of relevant sources of error during high-speed robotic fitting. The machining quality was quantified in terms of dimensional and geometric tolerance, chip formation and evacuation, burr formation, edge build-up, tool wear and surface damage. Statistical analysis of the experimental results reveals a strong dependence between part accuracy and drilling force. An experimental model was developed to represent and predict the cutting force during drilling and an accurate error prediction capability was distinguished. It was found that at high cutting speed and feed rate, the cutting force was the main source of error affecting the accuracy of the machined parts. Verification experiments are performed, and the results reveal that dimensional defects are significantly reduced by a heat treatment effect (90 HRE) and the thrust force decreases with an increase in cutting speed. The recommended cutting speed for robotic drilling is 6000 rpm with a feed rate of 0.15 mm/min. This study provides important technical guidance for improving the robotic drilling of aluminum alloy in practice.

## Keywords

industrial robot, high speed machining, aluminum alloy, design of experiments, desirability

## 1 Introduction

The industrial sector of material transformation uses the principle of material removal by cutting tool for machining. Generally, this method is based on the use of Computer Numerical Control (CNC) machine tools on which one or more cutting tools are installed. Machine tools are constantly evolving to meet the needs of companies that have increasingly strong flexibility constraints. In spite of these advantages which allowed improving the reliability of the production processes, to optimize the cycle time and to attenuate the loads on the operator, the recourse to this type of machine is subjected to several not negligible constraints such as a limited accessibility to some points in the space and a weak adaptability and flexibility of production. Currently, the manufacturing industry is a complex system whose activities meet technical, economic, human and social objectives. Thus, industrial robots have been efficient and sophisticated tools to perform repetitive and

intensive work. They are also used to replace the human operator in dangerous work environments. Nowadays, the presence of robots has become indispensable in some industrial sectors (automotive and aeronautics), as their use conditions the economic survival of companies [1]. This is especially true in the case of mechanical machining of metals such as aluminum, steel, titanium and other materials such as plastics and composites. Aluminum alloys have been widely used in the aerospace and automotive industries to replace weightier alloys. This is due to its superior properties of high specific strength, high corrosion resistance, good formability, recyclability and low manufacturing cost. In general, machining aluminum alloys is relatively easy compared to other metals. However, it can be difficult when it comes to drilling [2]. The high ductility of aluminum alloys often leads to the formation of long continuous chips and burrs at the entrance and exit of drilled

holes due to the work hardening effect [3]. The formation of burrs at the entrance and exit of holes can lead to difficulties in assembling the parts and can also lead to rejection of the parts. In addition, the competition in the global manufacturing industry is very high. The industrial need to change production techniques in order to meet the personalized demands of the products is constantly evolving.

Drilling is the most common material removal process used in the aerospace and automotive industries to create or enlarge holes through a component for assembly purposes. Tool wear is inevitable and severe in the machining of metal alloys. The involvement of worn tools in the machining process will reduce surface quality and increase production costs. In fact, failure at any point on the cutting edge will reduce the overall cutting performance of the tool and degrade the surface integrity. Therefore, it is necessary to provide for wear distribution in the different cutting edge [4]. However, traditional dry drilling significantly limits the improvement of machining efficiency and surface quality [5]. The mechanics of the drilling process have been extensively studied and several factors influence part accuracy, including robot accuracy, dynamic motion loads, thermal conditions, and cutting forces [6]. In this context, cutting force is an area of considerable research interest. Due to the high sensitivity and fast response of the cutting force signal to changes in cutting conditions [7–11]. The force signal can be processed for various tasks to optimize machine tool utilization, such as feed rate, tool wear, vibration, and force monitoring for tool breakage detection [6–15]. The use of industrial robots for machining processes instead of machine tools is widespread in various manufacturing fields, which contribute to perform automatically operation such as milling, drilling, grinding, deburring and polishing [16]. Many challenges have slowed down the adoption or sometimes inhibited the use of robots for machining tasks. While limited machining accuracy has been a major obstacle hampering the adoption of robotic machining systems [17, 18]. However, a discussion of various processes in which robots need to deal with significant process forces while fulfilling their machining task is necessary. Technical progress in robots have positioned them today as serious challengers to conventional machine tools in terms of precision, load capacity and flexibility for roughing and finishing machining operations [19]. Industrial robots have interesting speed performances but lower static and dynamic stiffness than machine tools. This evolution comes up against technical and technological constraints related to the devices set up to meet industrial requirements.

On the other hand, relatively reasonable amplitude of the machining forces, they induce on the robot which carries the spindle of machining of the deformations which can be not negligible with regard to the precision of desired realization. In addition, there is an appearance of vibratory phenomena that require the stopping of the process. This instability can cause a premature break of the tool or degradation by fatigue of the machine component. The deformable behavior of robots is linked to the deformable elements of their kinematic chain among which the reducers represent the most flexible element. Therefore, the use of industrial robots in the context of machining necessarily requires the control of the cut stability. Given these constraints, several industrial sectors have adopted industrial robots as an alternative solution to Computer Numerical Control (CNC) machine tools. Industrial robots are increasingly used for pre-machining operations that require high productivity. Therefore, the exploitation of industrial robots in the context of machining necessarily involves the control of cutting stability. Most of the researches work in robotic machining focuses on robot accuracy in terms of end-member placement accuracy and machining repeatability or vibration instability [20–26]. Therefore, it becomes important to be able to master their technology.

This research work is part of robotic drilling operations on aluminum alloys. The difficulties are generally manifested at the complexity level of integration and adaptation of these machines in processes of aluminum drilling. It aims to develop solutions to the technological problems associated with robotic machining by investigating the robotics adequacy for the drilling process. In this paper, the aim is to investigate the robotic drilling of an aluminum alloy with a focus on cutting forces, surface quality, dimensional and geometric tolerances. We investigate the characterization of the cutting effort as well as the interaction effort/dimensional quality according to several factors. The objective is to optimize the robotic drilling conditions with multi-performance characteristics using Taguchi's hybrid desirability approach.

## 2 Materials and methods

The drilling experiments were conducted using a KUKA robot (KR 500-2 MT with six axes) manipulating a high-speed SLF FS33-60/0.15 spindle with a KR C2 ed05 controller (Fig. 1). The KR 500-2 MT is a standard robot for a payload of 500 kg, a process force of up to 8,000 N and a reach of 3,326 mm. standard KUKA controller and software ensure reliable production results. The spindle

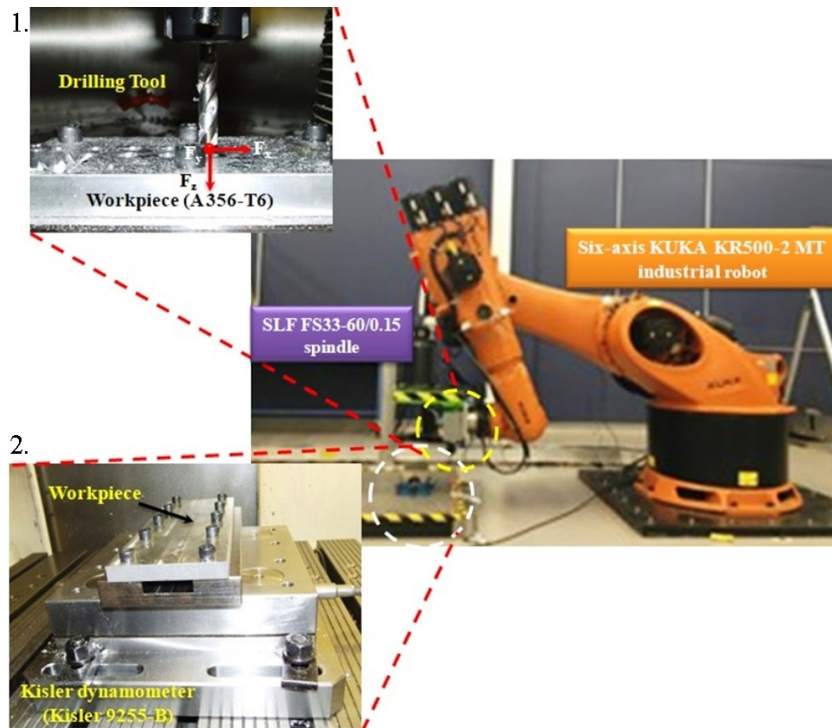


**Fig. 1** In the experimental setup used during the drilling tests, the KUKA robot manipulates a spindle; 1. Drilling tool used during the tests; 2. The block + 3-axis dynamometer assembly rigidly fixed to the positioning table

(SLF FS33-60/0.15) features the following characteristics: Maximum rotation of  $60,000 \text{ min}^{-1}$ , power of 170 W and torque of 6 N cm.

An uncoated high-speed steel twist drill was manually attached to the spindle and would be used to drill an A356 aluminum alloy block (3/8 inch truncated drill with  $118^\circ$  tip angle, Fig. 2). It should be noted that similar drilling tools were used during the testing to ensure reliability in the geometry and properties of the tools used (Fig. 1). The same coordinate system and robot configuration were kept for all drilling tests. The robot is positioned in a relatively folded configuration as shown in Fig. 1.

The distance between the robot base and the tool is 1839.43 mm and the drilling direction is parallel to the linear axis. The joint angles at the starting position of the robot are shown in Table 1.



**Fig. 2** Uncoated high-speed steel twist drill used for drilling A356 blocks

An aging heat treatment is applied to improve the strength and hardness of  $300 \times 100 \times 20 \text{ mm}^3$  size blocks of A356 alloy that were received in an as-cast condition ( $T_0$ ). These blocks underwent solution heat treatment "SHT" at a temperature of  $540 \text{ }^\circ\text{C}$  for 8 hours ( $T_4$ ). Then, the blocks were dipped in hot water ( $60 \text{ }^\circ\text{C}$ ) followed by artificial aging at  $155 \text{ }^\circ\text{C}$  ( $T_6$ ) and  $220 \text{ }^\circ\text{C}$  ( $T_7$ ) for 5 hours. For the measurement of micro-hardness, a Digital Micro-hardness Tester FM-1 was used. The hardness values obtained were 57, 76 and 90 HRE for A356-T4, A356-T6 and A356-T7 respectively (Table 2). These blocks were mounted on a three-axis dynamometer (Kistler 9255B table) using a hexagonal screw to properly quantify the robot's ability to drill under different cutting conditions. The assembly is rigidly attached to the positioning table (Fig. 1).

**Table 1** Joint angle at the starting position of the robot

Linear axis	Joint 1	Joint 2	Joint 3	Joint 4	Joint 5	Joint 6
436.8 mm	$88.35^\circ$	$-18.02^\circ$	$115.48^\circ$	$180.69^\circ$	$97.97^\circ$	$-0.3^\circ$

**Table 2** Typical mechanical properties of A356 alloy block

Property	A356		
	$T_4$	$T_7$	$T_6$
Tensile strength, $\sigma_b$ /MPa	150	234	200
Yield Strength, $\sigma_{0.2}$ /MPa	88	205	165
Elongation, $\delta\%$	4.0%	3.5%	2.0%
Hardness, HRE	57	90	76

The cutting force signals were then amplified and analyzed using the 48 KHz sampling rate. The raw cutting force data were exported to Matlab for further analysis and no filters were applied to the force signals. The average forces generated during the drilling of each hole were calculated in the time period corresponding to the first contact of the drill with the block surface and its complete retraction at the end of the drilling cycle.

The drilling experiments were conducted at different cutting speeds and feed rates. To formulate the relationship between the drilling responses and the cutting parameters and their interaction effects, a full factorial experimental design was used to construct the experiment matrix. For this purpose, three levels of cutting speed and feed rate were used. The factors studied and their levels are summarized in Table 3. The drilling tests were replicated three times for each condition. A total of 81 experiments were conducted to complete the study. The mean values of the recorded responses were used for the experimental analysis.

The diameter, circularity and cylindricity of the drilled holes were obtained using a Mitutoyo CRYSTA type three-dimensional measuring machine (CMM) ( $1600 \times 3000 \times 1100 \text{ mm}^3$ ) with special balancing. The measurements were repeated three times and the average value was used in the experimental analysis. To study the surface texture of the drilled holes, the specimens were ultrasonically cleaned in an ethanol bath. The arithmetic surface roughness  $Ra$  was recorded at four different positions and the measurements were repeated twice at each point using the Mitutoyo SJ 400 profilometer.

### 3 Results and discussion

#### 3.1 Experimental design and results

Fig. 3 (a), Fig. 4 (a) and Fig. 5 (a) show an example of thrust force signals ( $F_z$ ) obtained during dry drilling. It is evident that we obtain signals with substantially comparable force profiles. An analysis in the time and frequency domain of the experimental data of thrust forces collected

**Table 3** Drilling process parameters

Variable parameter		Low limit	Intermediate	High limit	Levels
Speed	rpm	2000	6000	10000	3
	m/min	60	180	300	
Tooth passing frequency	Hz	33.33	100	166.66	
Feed rate	mm/rev	0.015	0.15	0.35	3
Material hardness	HRE	57	76	90	3

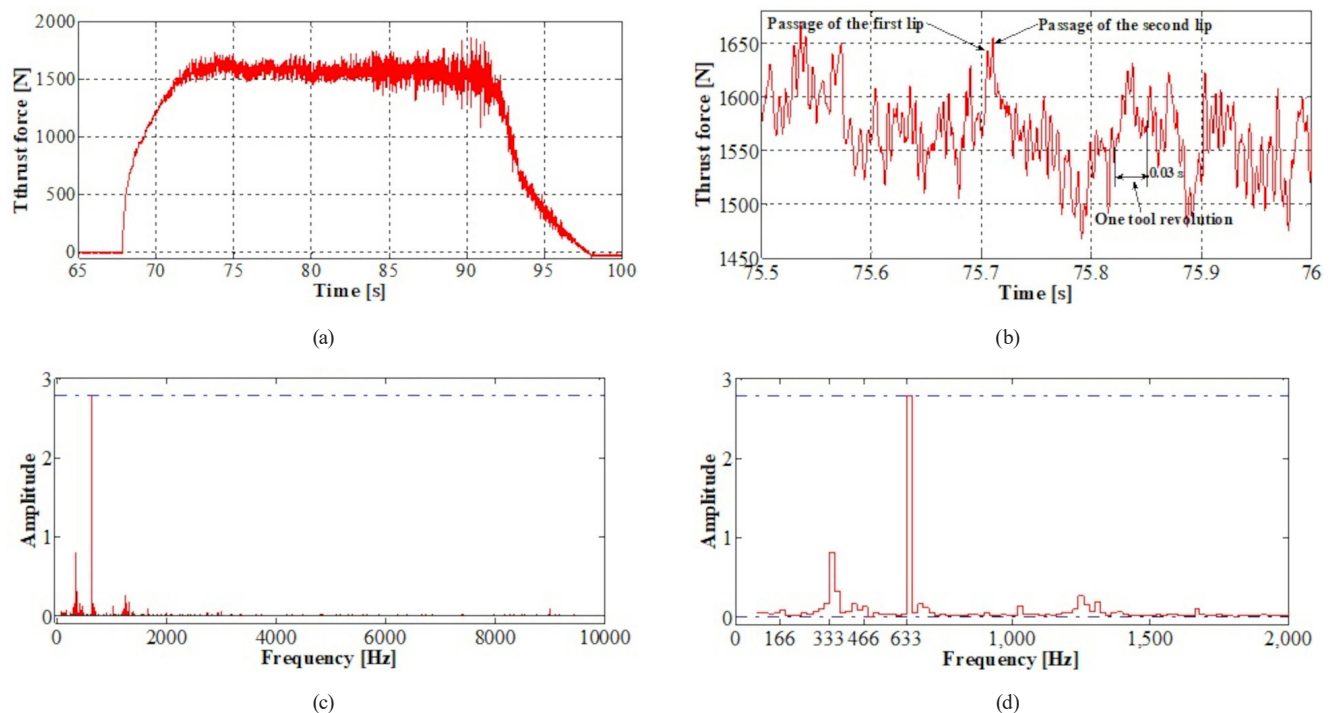


**Fig. 3** Thrust force in the time and frequency domain during robotic drilling at a speed of 2000 rpm and a feed rate of 0.35 mm/rev:

(a) Thrust force signals obtained during dry drilling; (b) Zoom in on the stability period of the thrust force; (c) FFT of the instantaneous thrust forces during the stability period; (d) Zoom in on the FFT plots

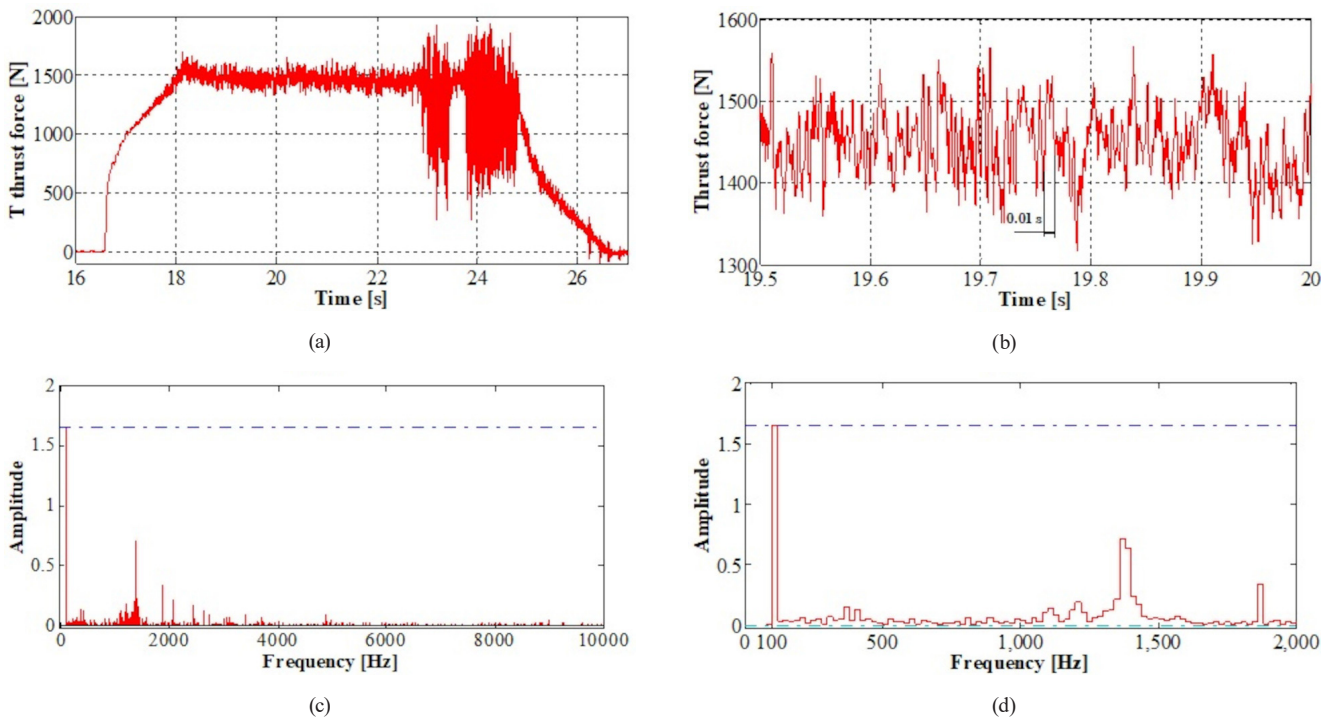


**Fig. 4** Thrust force in the time and frequency domain during robotic drilling at a speed of 6000 rpm and a feed rate of 0.35 mm/rev: (a) Thrust force signals obtained during dry drilling; (b) Zoom in on the stability period of the thrust force; (c) FFT of the instantaneous thrust forces during the stability period; (d) Zoom in on the FFT plots

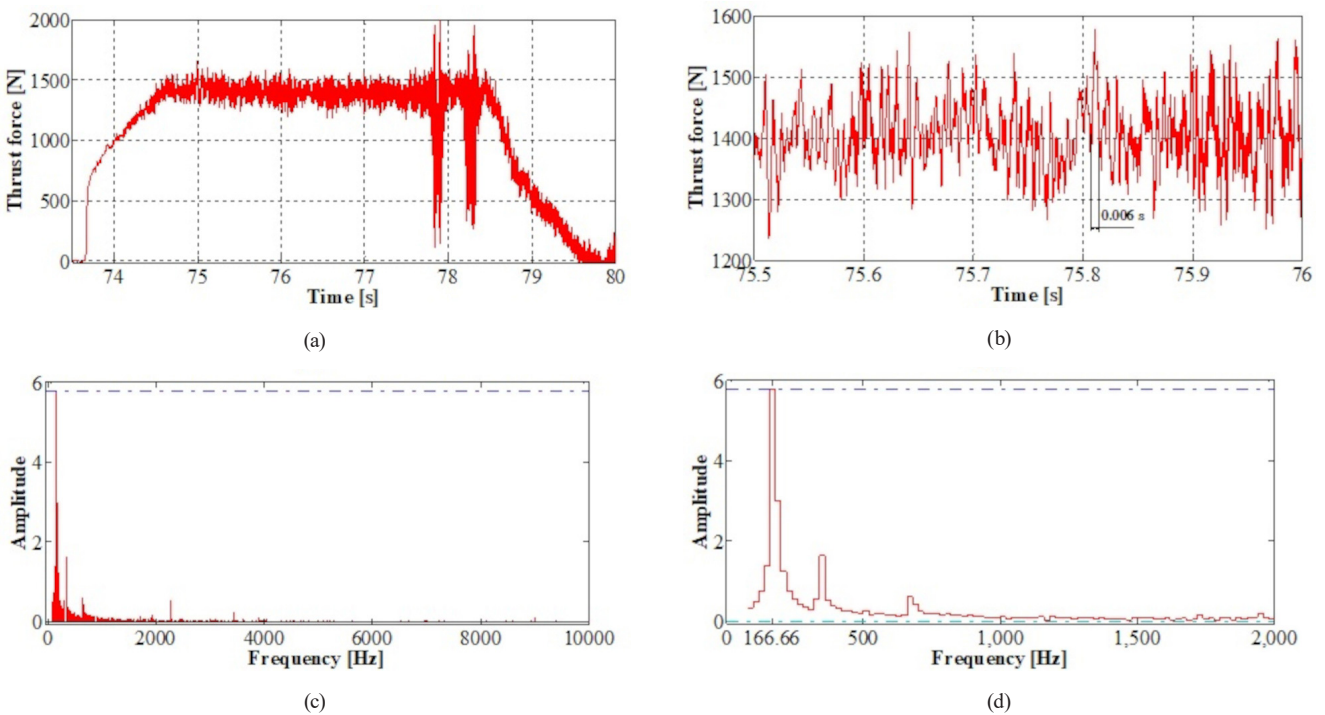


**Fig. 5** Thrust force in the time and frequency domain during robotic drilling at a speed of 10,000 rpm and a feed rate of 0.35 mm/rev: (a) Thrust force signals obtained during dry drilling; (b) Zoom in on the stability period of the thrust force; (c) FFT of the instantaneous thrust forces during the stability period; (d) Zoom in on the FFT plots

under different drilling conditions has been performed. Each revolution of the tool brings each cutting edge into contact with the material once. This interrupted cutting pattern causes the force on the cutting edge to fluctuate.

This interrupted cut contributes to vibration and leads to the resulting drilling errors. To verify the significant presence of interrupted drill cut and possible anomalies in the data acquisition during the drilling process, a zoom in on

the stability period of the thrust force was performed and presented in Fig. 3 (b), Fig. 4 (b) and Fig. 5 (b) and the frequency of cutting-edge passage was identified. These values show a peak in the thrust force for each edge, and the height of the peaks is not the same due to cutting interruption errors and other phenomena generated by the tool. The Fast Fourier Transform (FFT) is a powerful technique commonly used in signal analysis to detect periodicity and obtain the frequency components of a signal hidden in noise. Graphs representing the FFT of the instantaneous thrust forces during the stability period are reported in Fig. 3 (c), Fig. 4 (c) and Fig. 5 (c) respectively. Referring to Figs. 3 (c), 4 (c), 5 (c), it clearly indicates that the instantaneous thrust forces are the combination of forces at different frequency values. Zooming in on the FFT plots reveals that the tooth passage frequency is 100 Hz to 166 Hz for the rotational speed of 6000 rpm and 10,000 rpm respectively (Fig. 3 (d), Fig. 4 (d) and Fig. 5 (d)). These frequencies are in good agreement with the fundamental cutting-edge passage frequencies presented in Table 3.

Moreover, the FFT results also show that other sources of error introduce harmonic frequencies that are multiple of the cutting-edge frequency (two to four times the main frequency). Certainly, industrial robots are systems composed of several mechanical parts and mostly use gears to amplify the torques produced by their motors. However, the use of gears introduces non-linear and periodic errors in the operation of the amplification mechanism. Radial eccentricity, axial oscillation, tooth-to-tooth contact and gear tooth profile are sources of error in the operation of the industrial robot. In general, low-frequency components are mainly subject to eccentricity, wobbling in the bearing guides and gear misalignment. Abrupt changes or high frequency components are mainly subject to tooth-to-tooth contact and errors caused by ball-bearings [27]. During our tests, all robot joints rotate simultaneously, and more than 20 gears are involved in the drilling operation.

In addition, each gear has its own characteristics, it also produces specific signals. This describes the strong dependence of the robot stiffness on the cutting forces.

Also, the machining process contributes with its own unavoidable error such as tool runout which also contributes to produce uneven cuts with vibration risk. Tool runout leads to content in the drilling signal that is synchronous with the spindle speed. The signals overlap significantly and are combined by random noise, the situation becomes more complicated, and at this point it is very difficult to identify the frequency components by examining at the original signal. Despite this, the harmonic frequencies that are multiple of the cutting-edge pass frequency are certainly the frequencies due to tool runout in the absence of disturbances.

In this study, we used an average value of the thrust force. The results obtained are presented in Fig. 6, which describes the evolution of the thrust force ( $F_z$ ) for the different feed rates during robotic drilling (increase or decrease). The forces are amplified at a much higher magnitude when the feed rate is extremely high. Thus, it is observed that the force evolves almost linearly. In addition, the maximum force obtained when drilling at low rotational speed and high feed rate. These forces can cause a deflection of the robot spindle. It was also found that with the different hardness values, the average thrust force values remain very close. It should also be noted that the difference between the forces is substantially constant ( $\approx 600$  N) when changing the feed rate value. In addition, the variation of the thrust force is smaller with respect to the rotational speed ( $\approx 100$  N). In robotic machining processes where material is removed by mechanical action such as drilling, controlling the thrust force could significantly improve the stability and capability of the process. The greater the thrust force applied to the cutting tool, the greater the possibility of robot deflection. So, for good stability and process capability, the feed rate should be correlated with the rotation speed to minimize the thrust force.

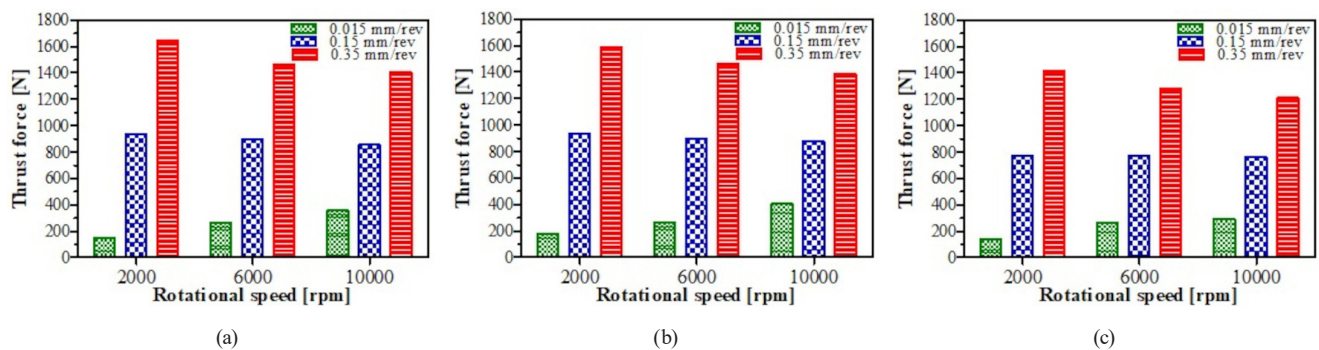


Fig. 6 Average value of thrust forces for all drilled holes: (a) Material hardness 57 HRE; (b) Material hardness 76 HRE; (c) Material hardness 90 HRE

### 3.1.1 Direct effects on the thrust force

Fig. 7 shows the direct effect of all the factors studied on the average value of the thrust force. The main objective is to show which factors have the maximum effect on the studied response ( $F_z$ ). Any increase in the cutting parameters leads to a change in the thrust force. The direct effect of each factor immediately highlights the important factor which is the feed rate. An increase in feed rate results in an increase in thrust force. Changing from a rigid material to a hard material decreases the thrust force. Rotational speed has a much smaller effect on the thrust force.

### 3.1.2 Pareto chart

The study of the influence of the parameters consists in determining the combination of factors that would increase the thrust force ( $F_z$ ). The Pareto diagram allows us to determine the influential factors in order of decreasing contribution. The reading of the Pareto diagram (Fig. 8) highlights the predominance of the feed rate factor on the thrust force. Thus, it can be seen that the three factors feed rate, material hardness and the interaction between feed rate and rotation speed alone explain more

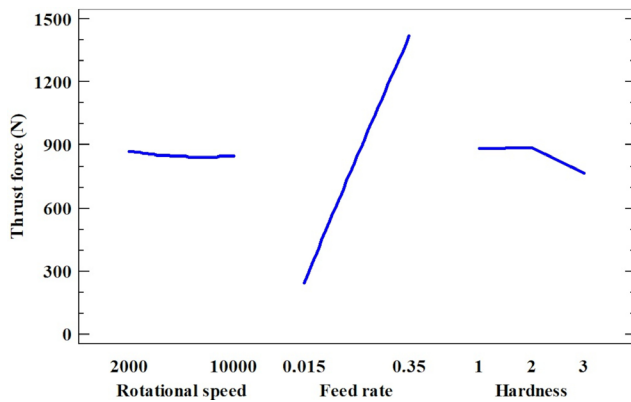


Fig. 7 Main effects plot for thrust force ( $F_z$ )

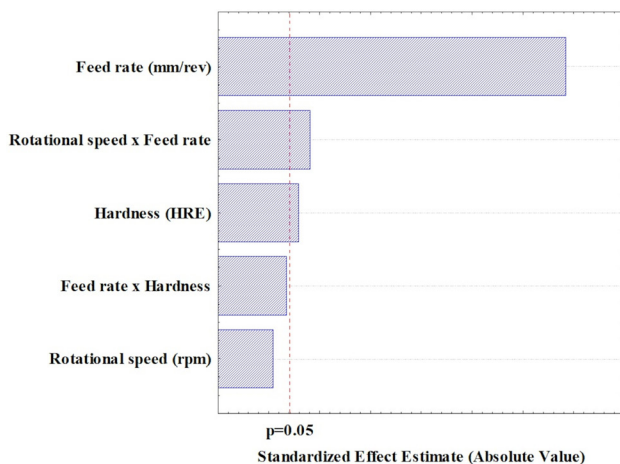


Fig. 8 Pareto chart of normalized effects for the thrust force ( $F_z$ )

than 95% of the variability of the response. The contribution of the rotational speed is masked because their influence is small. Thus, the factors feed rate and material hardness seem to be the ones to control to minimize the thrust force. The analysis of the direct effects on the response, their interactions and the order of contribution allowed us to distinguish the great influence of the feed rate and the material hardness on the thrust force.

### 3.1.3 Analysis of variance

Analysis of variance (ANOVA) allows us to study the main effects of the independent parameters, as well as their interactions, in order to know their combined effects on the dependent response. From the significant variables and their interactions, a multiple regression analysis will allow establishing an empirical model with a coefficient of determination  $R^2$ . Table 4 presents the ANOVA statistical results for drilling thrust force. This analysis of variance was performed for a significance level of 5%, i.e., for a confidence level of 95%. The last column of Table 4 shows the contribution of the factors (in %) to the total variation, indicating the degree of influence on the result. The results show that the feed rate is the factor that represents the greatest effect on the variation of thrust force, explaining 94.9% of the contribution. The interaction between rotational speed and feed rate is found to be significant in Table 4 (1.845%), and therefore, the presence of rotational speed in the regression model is found to be necessary (0.016%) and feed rate should be correlated with rotational speed. Also, the hardness effect was with a contribution of 1% on the thrust force. Then, the interaction between the feed rate and the material hardness was with a contribution of 0.343%. On the other hand, the other interactions present very low percentage contributions on the variation of thrust force.

Table 4 ANOVA results of the thrust force variance

ANOVA; Var.: Thrust force (N); R-sqr = 97.66%, 33-level factors, 3 Blocks, 27 Runs						
	SS	df	MS	F	p-value	(%)
Rotational speed (rpm)	1057	1	1057	0.1477	0.704562	0.016
Feed rate (mm/rev)	6095541	1	6095541	851.8586	0.000000	94.92
Hardness (HRE)	61424	1	61424	8.5840	0.008004	0.956
$N \times f$	118496	1	118496	16.5600	0.000550	1.845
$f \times HR$	22055	1	22055	3.0822	0.093731	0.343
Error	150267	21	7156			
Total SS	6421501	26				

### 3.1.4 Regression model

Regression analysis was used to develop the regression model for the thrust force response. The processing of the experimental results obtained in Table 4 allowed the determination of a statistical model, expressing the relationship between the different factors of rotational speed ( $N$ ), feed rate ( $f$ ), material hardness ( $HR$ ) during robotic dry drilling of A356 aluminum. In order to establish a model to explain the response, the quality of the model must first be verified. The statistical test that measures the quality of the modeling is the multiple correlation coefficients  $R^2$ , which expresses the ratio of the variance explained by the model to the total variance. To determine which parameters are most influential on the dependent responses in our empirical model, we compared  $R^2$  following the step-by-step method used manually, which starts from the complete model and at each step the associated variable with the largest  $p$ -value (Table 4) is eliminated from the model. The coefficient of determination of the model is high and converges to unity indicating a good agreement with the experimental results. Table 4 shows the coefficient of determination values ( $R^2 \approx 97.66\%$ ) of the proposed model, which indicate a good correlation between the predicted and experimental robotic drilling data. The results compiled in Table 4 show that all the variables and their interactions have a significant effect on the dependent variable thrust force. This method allowed us to classify according to the degree of fit and choose the required model, which is in Eq. (1):

$$F_z = 223.94 + 5460.56f - 0.73HR - 0.14f \times N - 15.36f \times HR + 65.37. \quad (1)$$

The analysis of the mathematical model makes it possible to define more precisely the evolution as well as the degrees of the various factors influencing the increase in the thrust force. To this end, the analysis of the different factors shows that the greatest influence is reserved for the feed rate, followed by the hardness of the material, while the rotation speed has a negligible influence, which is why it does not occur in the model. The validation of the results given by the model consists in examining if the assumptions made at the beginning of the experimental design are well verified. In our case, all the combinations of our experimental design are well tested. We were therefore able to calculate all the interactions. However, the hypothesis of linearity of the response remains to be verified. To do so, if the distribution of the predicted values is normal to the observed values, the plotted points must be aligned on a line. If an effect does not satisfy

this condition, it means that it deviates from normality and is therefore likely to be insignificant. The corresponding factor or interaction may therefore be insignificant in this case. The predicted thrust force values show that the plotted points are nearly aligned on a straight line (Fig. 9). The predicted forces are close to the normal line and are therefore normally distributed. The residuals between the measured and predicted values are less than 5%. Consequently, the values that deviate from the straight line are due to measurement errors and to factors that have been eliminated from the proposed model.

### 3.1.5 Response surface

The graphical representation of the regression model equation allows us to illustrate the variations in response and eventually identify the areas of the experimental field in which the thrust force is maximum or minimum. The response surfaces (Fig. 10) concretize the variation of thrust force as a function of the different factors of rotational speed ( $N$ ), feed rate ( $f$ ) and material hardness ( $HR$ ) during A356 robotic drilling. From Fig. 10, it can be seen that an increase in thrust force occurs for the different cutting conditions. The feed rate has a significant effect on the increase in thrust force, regardless of the rotation speed and the material hardness used. Also, it is observed that material hardness leads to higher thrust force at high rotation speed. It was also found that the effect of material hardness on the force profile was similar as that of rotation speed. In this study, the minimum is given by a rotational speed ( $N = 2000$  rpm), feed rate ( $f = 0.35$  mm/rev) and for a hardness (57 HRE). The main conclusion of these response surface is that there are combinations between

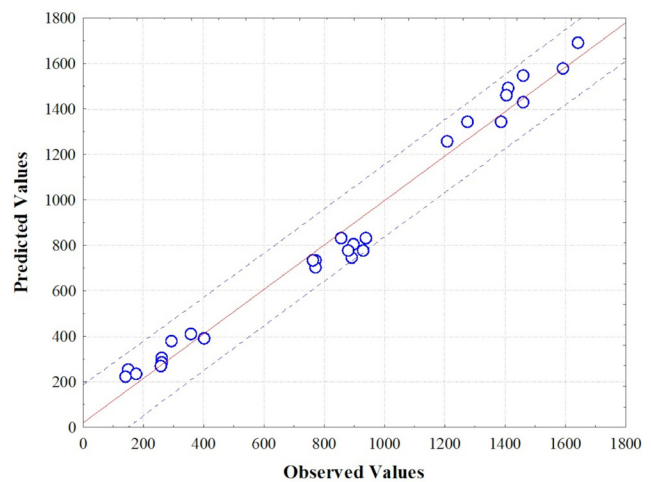
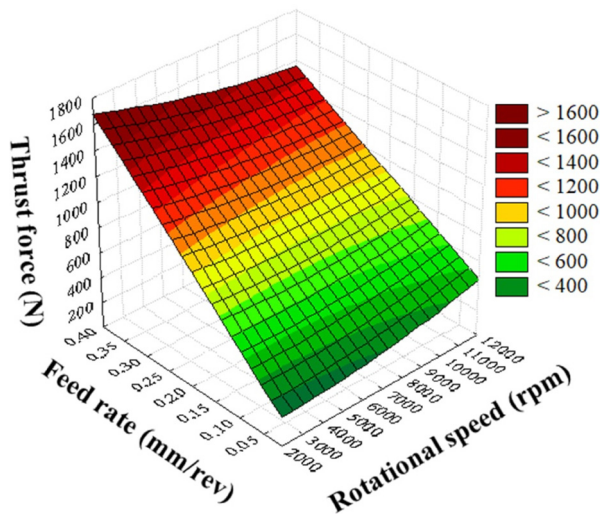
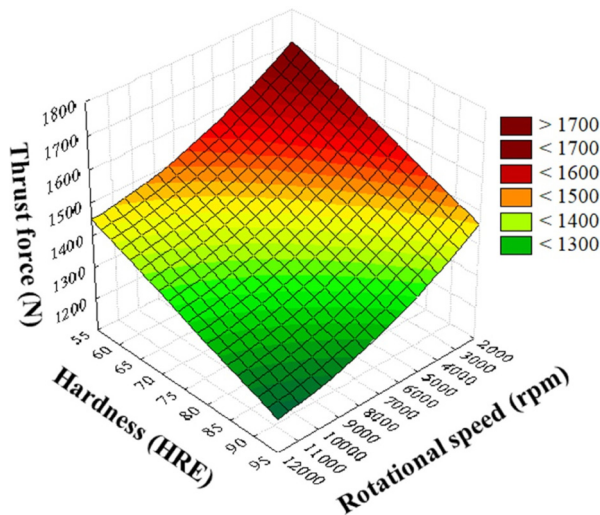


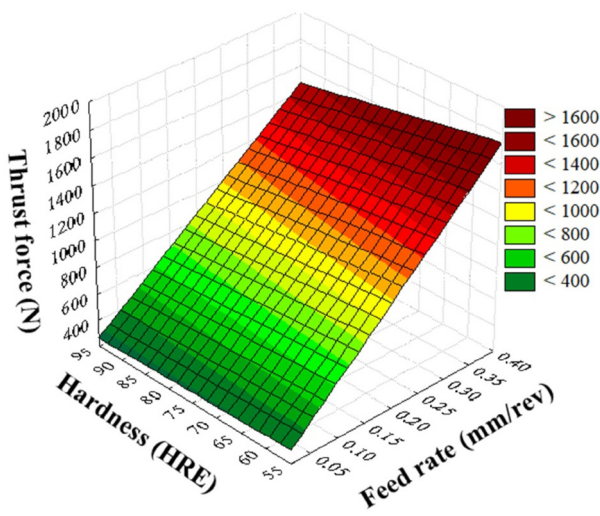
Fig. 9 Adequacy of the proposed prediction model with the observed values of the thrust force



(a)



(b)



(c)

**Fig. 10** Thrust force variation as a function of different factor interactions:  
 (a) Feed rate and rotation speed; (b) Hardness and rotation speed;  
 (c) Feed rate and material hardness

the different factors ( $N \times f, N \times HR, f \times HR$ ) for which the thrust force is low. In the considered experimental area, the response surfaces underline the major importance of the feed rate factor on the thrust force level achieved by the combination between the rotation speed and the material hardness. The hardness factor of the material also contributes significantly to the achievement of a low force, but to a minor degree compared to the interaction between feed rate and material hardness, which can also be explained by the hardness range explored which are relatively small. This leads us to conclude that the feed rate factor is of primary importance in the management of the thrust force.

### 3.2 Discussions

#### 3.2.1 Dimensional and geometric tolerances

The objective of robotic drilling is to obtain a hole that satisfies specific dimensional and geometric requirements. It is therefore necessary to verify that the conditions studied respond to these requirements. Once the robotic drilling was completed, the drilled holes were inspected in the metrology laboratory using a coordinate measuring machine (CMM). After measuring the average diameters (Fig. 11), the circularity and cylindricity were calculated. The results of the inspection are presented in Fig. 12. In these measurements, the ability to drill A356 aluminum alloy using the robot was evaluated in terms of hole diameter accuracy. The drilled holes quality is directly related to the circularity and cylindricity value of the holes. Consequently, the calculated diameter and circularity will be affected by many error sources with different shapes and frequencies.

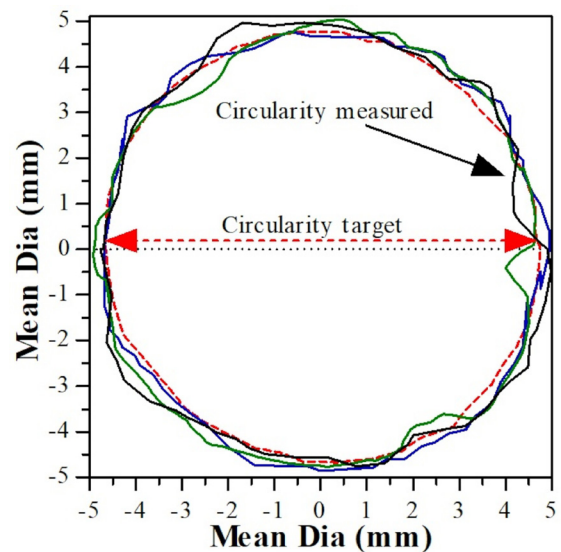


**Fig. 11** Measured circularity with a drilling depth of 20 mm

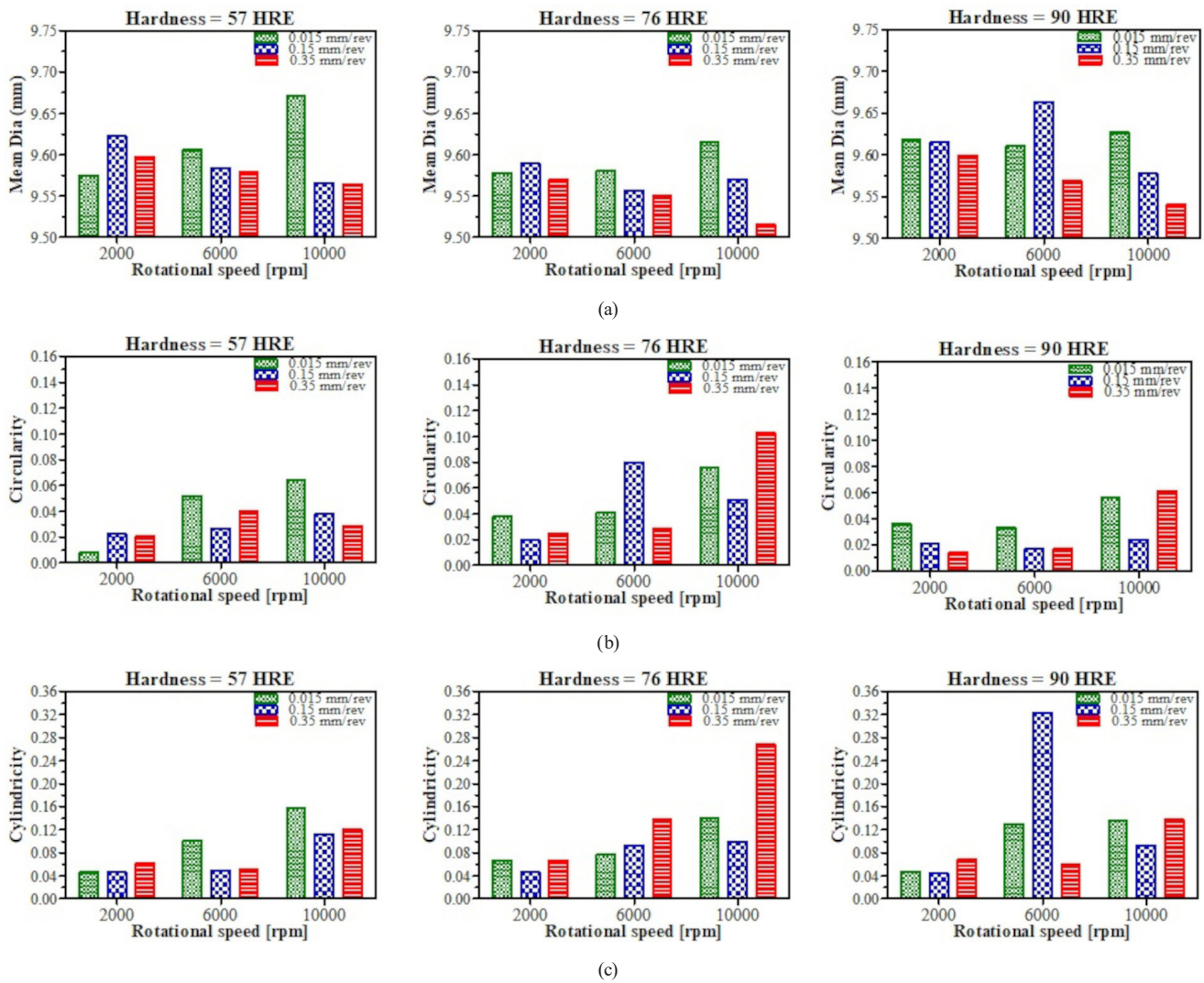


Fig. 12 Results of (a) average diameter deviation; (b) circularity and (c) cylindricity of holes for different cutting conditions

Since the robotic drilling in this work is mainly used for the passage of fasteners (bolt, rivet ...), the diameter of the through-hole is often associated with so-called envelope tolerances. The hole dimensions are characterized by a nominal diameter of 9.525 mm, a tolerance width of IT8 and a tolerance position of H8 according to ISO for holes with sliding fit (IT8 = 27 microns) [28, 29]. H9 hole tolerances with poor hole quality is obtained for a very low rotational speed which caused high plastic deformation (IT9 = 43 microns). Deviations between the nominal and the achieved diameter can result from a variety of sources. The non-conformity is due to the robotic drilling stability which generates thrust forces causing the deviation of the tool axis (tool runout). Also, it can be a phenomenon of chip evacuation and thermal shrinkage (dry drilling). In Fig. 6, it was found that the average value of the thrust forces increases with increasing feed rate. On the other hand, the linear relationship observed in Fig. 12 (a) during

robotic drilling indicates that the degree of increase or decrease in the average diameter deviation was related to the rotation speed. Although the average thrust forces increase with increasing feed rate, the results show that robotic drilling at medium feed rates and high material hardness provides a more accurate tolerance than drilling at low material hardness (Fig. 12 (b)). In addition, the cylindricity shows a clear relationship between rotational speed and material hardness (Fig. 12 (c)).

### 3.2.2 Chip formation and evacuation

The drilling process can be compared to milling and turning, but the requirements for chip formation and evacuation are more severe for drilling. In our robotic drilling tests, the shortest possible drill bit was used to reduce deflection and vibration. Fig. 13 shows similar chip morphologies depending on the feed rate applied. Indeed, it can be seen that the drilling produces a conical helical

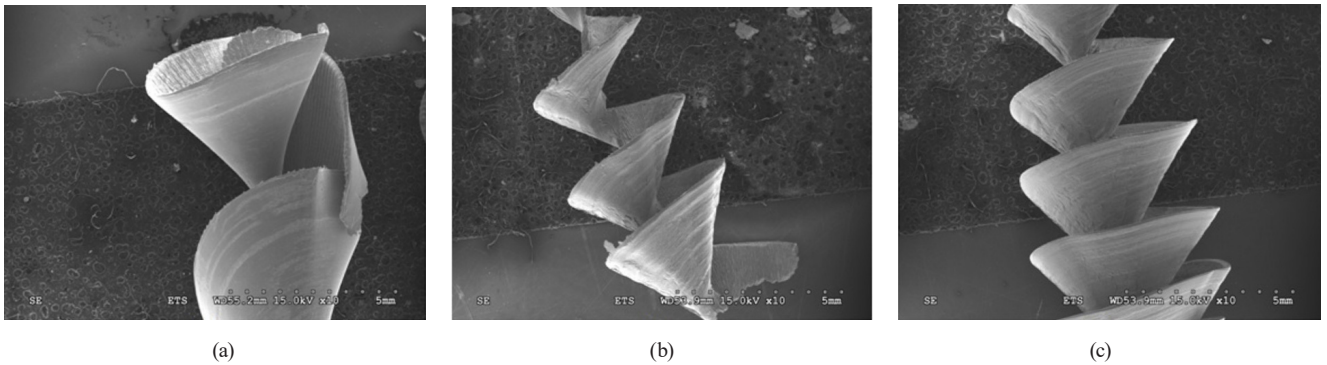


**Fig. 13** Variation in chip formation under different feed rate when drilling A356 at 6000 rpm and 57 HRE:  
 (a) 0.015 mm/rev; (b) 0.15 mm/rev; (c) 0.35 mm/rev

chip with a small or large pitch. The compactness obtained minimizes the length of the chip and allows the chip to optimally occupy the entire flute of the drill.

Long chips can cause jamming in the drill flutes. At high feed rates, the morphology of the chips generated is found to be quite chaotic, with tendencies towards tangling (Fig. 14). In addition, it was also observed that the thicker and stiffer chip section obtained when drilling at high feed rates (Fig. 13 (c)). This suggests problems with evacuation.

To do this, the chip must have both a length and a morphology adapted to the tool. If this is not the case, poor chip removal can lead to surface deterioration or tool breakage. For the process to be stable, the cutting conditions must be set to produce short chip shapes (Fig. 13 (a)).

After examining the chip morphology, we considered that segmented chips are typical of aluminum alloys, as shown in Fig. 15. The chips produced by robotic drilling A356 at a hardness of 90 HRE show many small cracks

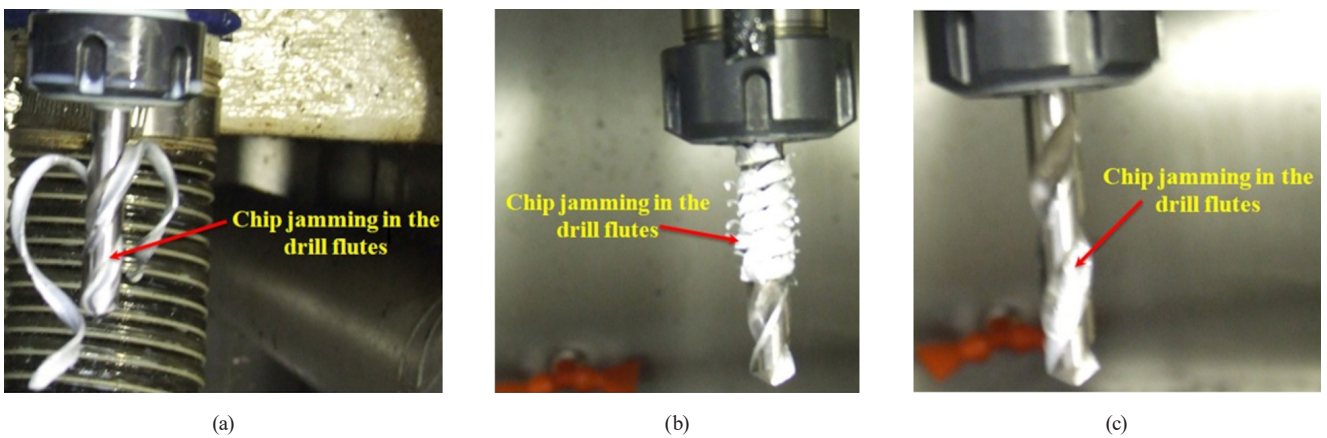


**Fig. 14** Long chips that cause blockages in the drill flutes:  
 (a) Material hardness 57 HRE; (b) Material hardness 76 HRE; (c) Material hardness 90 HRE

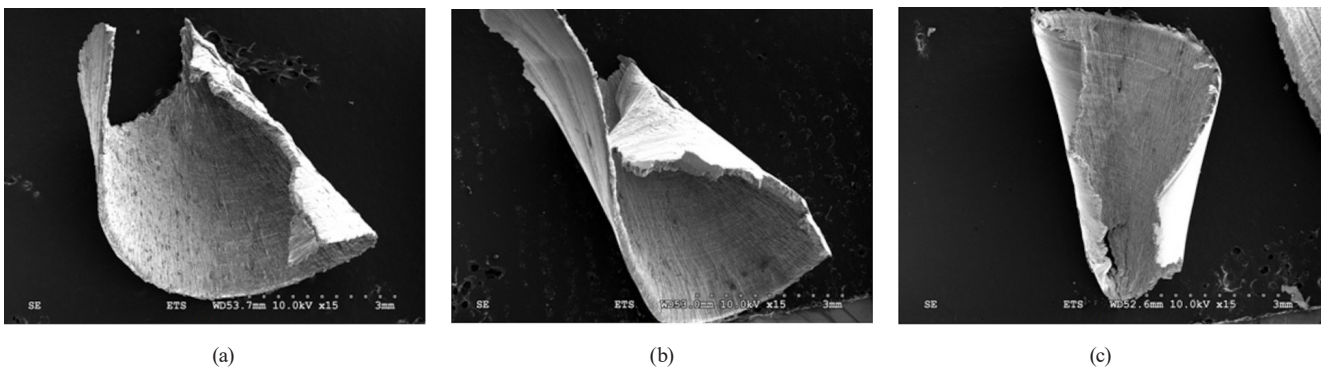


**Fig. 15** Variation in chip formation under different hardness when robotic drilling A356 at 6000 rpm and 0.015 mm/rev:  
 (a) Material hardness 57 HRE; (b) Material hardness 76 HRE; (c) Material hardness 90 HRE

that characterize brittle fracture (Fig. 15 (c)). In contrast to a hardness of 57 HRE which is more ductile, the chip formation does not reveal this type of cracking (Fig. 15 (a)). At the minimum feed rate, the chip structure has a high plastic deformation and is more deformed and elongated. Chip fragmentation and evacuation become stable when the chip fracture is brittle at high rotation speed and low feed rate (Fig. 15 (c)). Because high rotational speed results in less curled chips due to less friction and high feed rate produces thicker and stiffer chips.

### 3.2.3 Burrs formation

Fig. 16 shows the type of burr generated at different material hardnesses when robotic dry drilling of alloy A356. The results show that hardness has a significant effect on the formation and size of burrs. The burr defect is characterized by a localized excess of material on the hole transverse edge. During the drilling process, as the tool approaches the surface exit, the material volume remaining to be cut decreases. Below a minimum thickness, the material will start to deform plastically from the

transverse edge towards the cutting edge under the action of the thrust force. When the drill opens, this deformed material will be pushed away from the workpiece in such a way that it will no longer be in the path of the tool edges and will therefore not be cut (Fig. 16). Observations have shown that the burrs generated on the entry side are much smaller than those on the exit side. As a result, most of the burrs are on the exit surface while the entry surface of the hole has little or no burrs.

In addition, it was found that for different rotation speeds and feed rates, the most common type of burr observed was a homogeneous burr of uniform thickness (Fig. 17). The appearance of this phenomenon depends on several parameters, including the thrust force and the material ductility. It is noted that an increase in the material ductility will result in the formation of larger burrs. It can also be seen that this phenomenon increases as the thrust force (or feed rate) increases. In robotic drilling, burrs require additional deburring operations to facilitate re-assembly. Even if this defect can be corrected in most cases, it nevertheless generates additional production costs. Different

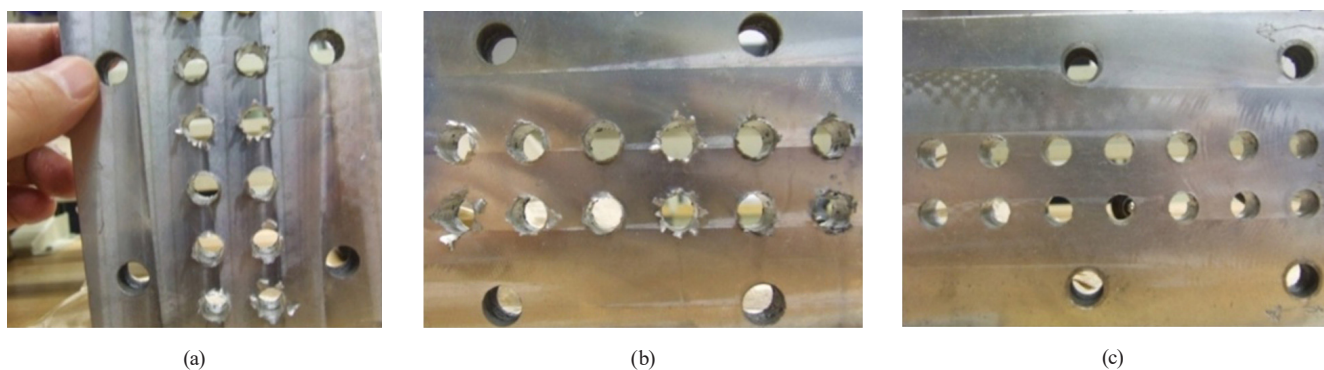


**Fig. 16** Material hardness influence on burr formation when robotic drilling of aluminum alloys A356 at 6000 rpm and 0.35 mm/rev:  
 (a) Material hardness 57 HRE; (b) Material hardness 76 HRE; (c) Material hardness 90 HRE

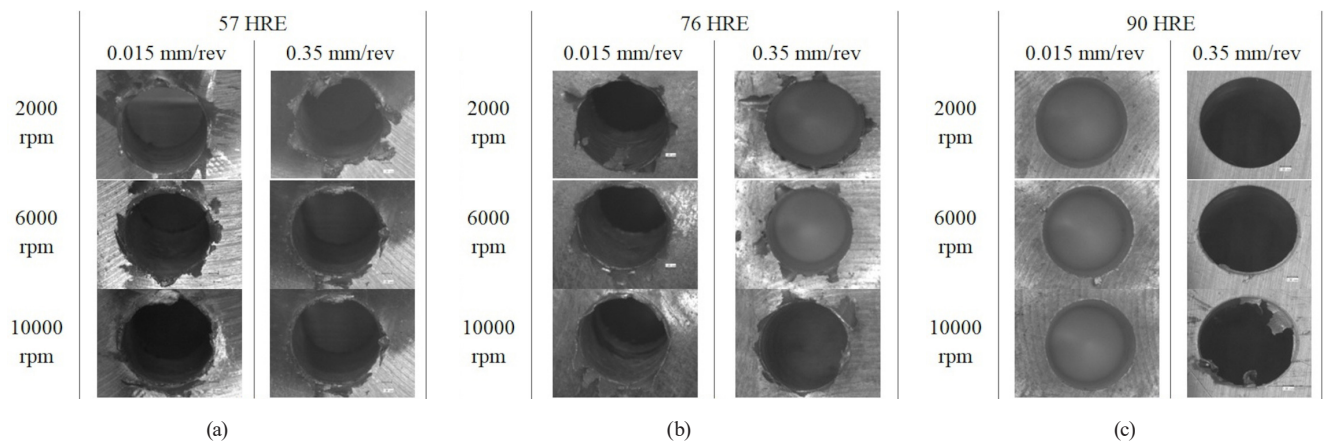


**Fig. 17** Material hardness influence on burr formation when robotic drilling of aluminum alloys A356 at different feed:  
 (a) Material hardness 57 HRE; (b) Material hardness 76 HRE; (c) Material hardness 90 HRE

strategies can be adopted during the robotic drilling process, such as using adaptive control of the thrust force and keeping it below a critical value in order to reduce the occurrence of burrs. Also, burr reduction can be achieved by selecting a low feed rate with a less ductile material obtained by heat treatment.

### 3.2.4 Built up edge chip formation and tool wear

In general, the cutting parameters and conditions, the tool type and the material nature being drilled are the three parameters governing wear. In the case of A356 at 57 HRE, which is generally soft and more ductile, it was found that for all rotation speeds, robotic dry drilling generated a higher thrust force mainly due to built up edge (BUE) on the drill bit (Fig. 18). They are located at the tip, the main cutting edge and the tool nose. The BUE phenomenon is manifested by the deposition of a mass of material on the cutting face, the edge and the skirt, modifying the initial geometry, the tool/chip contact and the cutting angle. As the built-up edge tends to grow, it becomes unstable and eventually breaks. As a result, the robotic drilling process becomes unstable.

Throughout our tests, similar drilling tools were used for each drilling operation to ensure consistency in the geometry and properties of the tools used. Fig. 19 shows an example of tool flank wear. In all the experiments carried out, the main form of tool failure in A356 drilling is flank wear (Fig. 19). The abrasive wear process in A356 drilling is not at all different from the usual tool wear process in metalworking. This is due to the presence of hard silicon particles in the drilled aluminum matrix. However,

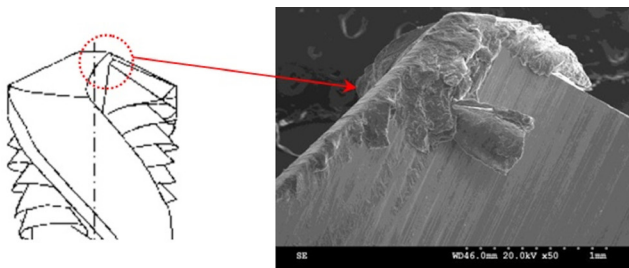


Fig. 18 Built-up-edge formation in tool flank

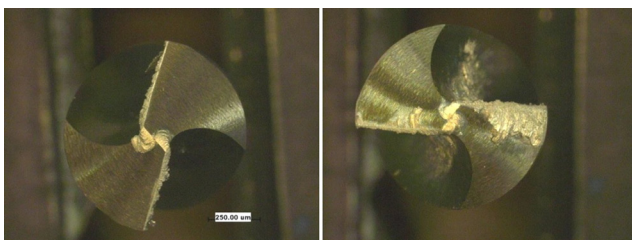


Fig. 19 Tool flank wear

the wear on the tool flank was insignificant at the cutting edge. This is the only wear mode present for all rotational speed, as these particles are not influenced by the relative tool/chip kinematics.

### 3.2.5 Surface finish and roughness index

The drill bit is inside the workpiece and is not visible during the operation. Robotic dry drilling produces highly deformed areas on the sidewall and damage that leaves spiral marks on the surface machined by the tool (Fig. 20). The surface finish of the drilled holes is a very important result on the parts performance and durability. The particular surface effects observed in robotic dry drilling can be explained by the phenomenon of chips being drawn against the side wall of the hole as the drill retracts. Also, reduced hole quality is due to poor chip evacuation at low rotation speed. It was also found that chip fragmentation is more difficult at high feed rates and mainly influences the surface finish and contributes to the hole quality. In addition, chip sealing in the drill flutes was observed to lead to less efficient chip evacuation. As a result of these disturbances (chip evacuation and jamming, insert edge, ...), the surface condition can become unpredictable and lead to dimensional variations during drilling. Therefore, the quality of drilling with a robot depends on many factors that influence the cutting force signals. In addition, the topography and texture of the drilled surface is used more as an indication of the variation in tool wear, tool vibrations detected directly on the robot components.

The surface roughness values ( $Ra$ ) of the drilled hole are shown in Fig. 21. They are measured parallel to the feed direction. It is obvious that the surface roughness depends on the machining factors used at each time, which is a complex problem in the robotic drilling process. Generally, the

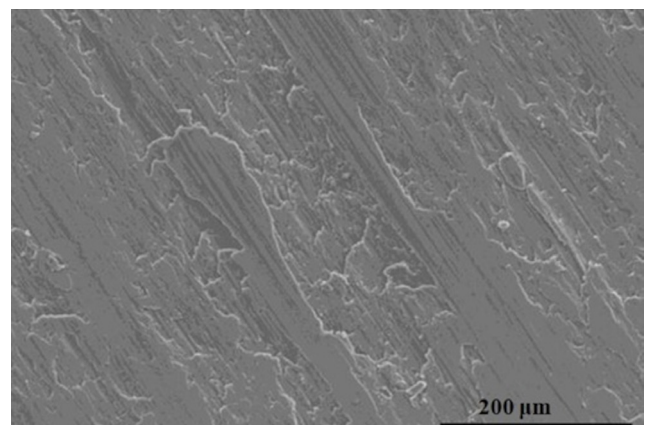


Fig. 20 Surface finish when robotic drilling of A356 with a hardness of 76 HRE, at 6000 rpm and 0.15 mm/rev

surface roughness is affected by two main factors: the feed rate and the tool geometry (cutting edge). From Fig. 21, it is confirmed that with an increase in material hardness, the surface roughness values ( $Ra$ ) are more shaped. Therefore, material hardness is a dominant parameter and has much more effect on  $Ra$ . The comparison between different feeds with the same tool shows that the higher feed rate increases the separation between the feed marks, which leads to an increase in the value of the geometric surface roughness. The feed rate has the main influence on the surface finish obtained. It has been found that the lowest feed values give a cheap finish due to the very low chip thickness which leads to poor surface formation. Asymmetrical roughness due to plastic deformation was observed when drilling the A356 at low rotational speed. Above a certain rotational speed value, the irregular roughness disappears. The surface roughness at low rotational speed is influenced by plastic surface deformation and BUE formation. The rotational speed is the parameter that has a great influence on the roughness due to the contribution of the processed material to the robotic machining process.

Finally, the criterion of the hole wall roughness depends essentially on the stability of the process and the good chips evacuation. The roughness qualification is acceptable if the value does not exceed 1.6 microns. Conformity with this geometric criterion can only be achieved by acting on the process/tool pair:

- On the robotic drilling process side, it is important to limit undesirable vibrations, spindle runout and to adapt the cutting parameters.
- On the tool side, the diameter of the drill bit allows the hole to be calibrated. It is therefore important, once the tool has been set, to prevent variations in edge geometry caused by wear or by the sticking of the removed material (seen when drilling aluminum parts).

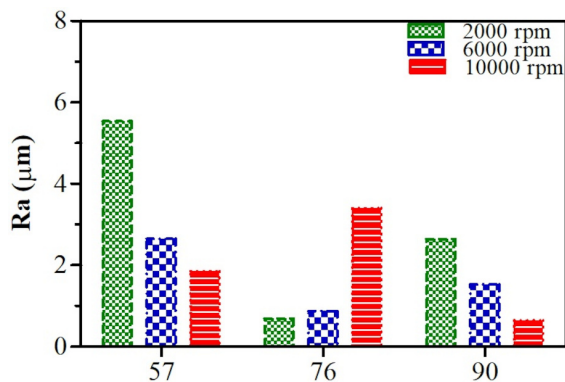


Fig. 21 Material hardness influence on surface roughness during robotic drilling of the A356 at 0.15 mm/rev

- Chip formation and chip evacuation are the main factors influencing hole quality in drilling (Figs. 14, 15).

### 3.2.6 Optimization of robotic drilling conditions

In general, the industry needs to produce parts with dimensional tolerances that are more important than generating a thrust force. Since each process response is important, it is necessary to optimize all these responses simultaneously, not one by one. In our optimization problem, the objective is to minimize geometry deviation and plot the expected circularity or cylindricity in the plane of rotational speed and feed rate. It is therefore necessary to find the levels of the input variables that allow the best compromise to be obtained. There are several methods of getting as close as possible to the minimum value required. One of these methods is to use the desirability function, proposed by Derringer and Suich [30], which introduces a global desirability criterion for the proposed input variables. By using this method, the optimization of several quality characteristic problems becomes simpler. This method uses an objective function, called the desirability function, and transforms the estimated response into a scale-free value, called desirability, which ranges from 0 to 1. The desirability value increases as the corresponding response increases. The factor setting levels with the maximum desirability value are considered the optimal parameters. Multiple response optimizations were applied to determine the global optimum and then to achieve the study objective of minimizing thrust forces and dimensional tolerance. According to the optimization analysis, it was observed that the highest desirability value ( $\approx 90\%$ ) is achieved in the test with the combination in Table 5.

When the number of response variables is small, the contour plots for each response can be superimposed to graphically show the optimum point (Fig. 22). These response plots for desirability show that at constant feed rate, desirability varies with changing rotation speed and material hardness. However, under all conditions, max desirability can be achieved at the low rotation speed and high feed rate, while min desirability is expected at the highest rotation speed and feed rate. In addition, it can

Table 5 Highest desirability value obtained in the test with the combination between rotational speed, feed and hardness

Properties	Values	Thrust force with the circularity
Rotation speed:	6000 rpm	$F_z = 770.96 \text{ N}$ Circularity = 17 $\mu\text{m}$
Feed rate:	0.15 mm/rev	
Hardness:	90 HRE	

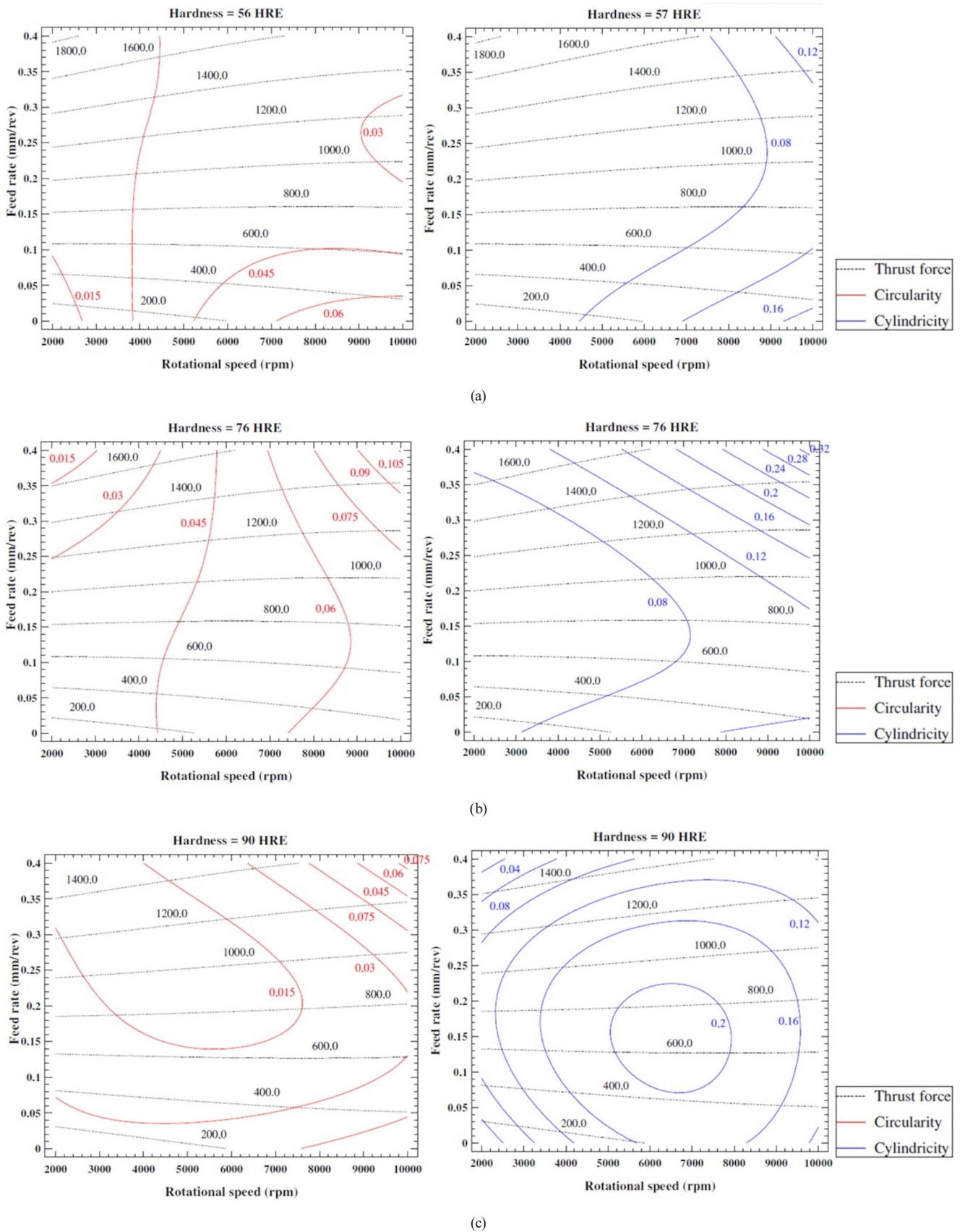


Fig. 22 Dimensional tolerances deviation as a function of thrust force for different cutting conditions:  
 (a) Material hardness 57 HRE; (b) Material hardness 76 HRE; (c) Material hardness 90 HRE

be seen that max desirability can be achieved by using a material with high hardness. The following graphs show the responses as a function of feed rate and rotation speed. In general, for the uncoated high-speed steel twist drill, drilling at low rotation speed (2000–6000 rpm) and high feed rate (approx. 0.3 mm/min) leads to a better tolerance according to ISO [28, 29].

#### 4 Conclusions

In this paper, we characterize robotic drilling in terms of cutting forces, dimensional quality and the interaction between them. This study shows that, regardless of the material being machined, the robot and its configuration, the degradation of dimensional drilling quality increases with increasing cutting forces. Minimizing the cutting force with the use of optimal cutting conditions improves the accuracy of the robot. In addition, the effect of low joint stiffness manifested itself in the degree of cutting force fluctuations that decrease the stability and repeatability of machining in mass production. Based on the experimental results, the following conclusions can be written:

- The FFT analysis of the instantaneous drilling forces during the steady state period shows a large number of peaks corresponding to the tooth passage frequency and its harmonics and to the tool runout frequency.
- A clear relationship between geometric deviation and drilling effort was observed.

#### References

- [1] Niku, S. B. "Introduction to robotics: analysis, control, applications", [e-book] John Wiley & Sons, 2020. ISBN 9781119527602 [online] Available at: [https://books.google.dz/books?hl=ar&lr=&id=rLfADwAAQBAJ&oi=fnd&pg=PR15&dq=%5B1%5D%09Niku,+S.+B.+Introduction+to+robotics:+analysis,+control,+applications.+John+Wiley+%26+Sons+\(2020\).+ISBN+9781119527602+\(epub\),+9781119527596+\(adobe+pdf\).+https://lccn.loc.gov/2019024970&ots=\\_v2rrr3lAn&sig=G-BbGR5dhg5vyfoOIHQYmSijIDA&redir\\_esc=y#v=onepage&q&f=false](https://books.google.dz/books?hl=ar&lr=&id=rLfADwAAQBAJ&oi=fnd&pg=PR15&dq=%5B1%5D%09Niku,+S.+B.+Introduction+to+robotics:+analysis,+control,+applications.+John+Wiley+%26+Sons+(2020).+ISBN+9781119527602+(epub),+9781119527596+(adobe+pdf).+https://lccn.loc.gov/2019024970&ots=_v2rrr3lAn&sig=G-BbGR5dhg5vyfoOIHQYmSijIDA&redir_esc=y#v=onepage&q&f=false) [Accessed: 02 June 2023]
- [2] Dahnel, A. N., Fauzi, M. H., Raof, N. A., Mokhtar, S., Khairussaleh, N. K. M. "Tool wear and burr formation during drilling of aluminum alloy 7075 in dry and with cutting fluid", *Materials Today: Proceedings*, 59, pp. 808–813, 2022. <https://doi.org/10.1016/j.matpr.2022.01.110>
- [3] Altintas, Y. "In-process detection of tool breakages using time series monitoring of cutting forces", *International Journal of Machine Tools and Manufacture*, 28(2), pp. 157–172, 1988. [https://doi.org/10.1016/0890-6955\(88\)90027-2](https://doi.org/10.1016/0890-6955(88)90027-2)
- [4] Mao, Z., Luo, M., Zhang, D. "Tool wear prediction at different cutting edge locations for ball-end cutter in milling of Ni-based superalloy freeform surface part", *The International Journal of Advanced Manufacturing Technology*, 120(5–6), pp. 2961–2977, 2022. <https://doi.org/10.1007/s00170-022-08790-4>
- [5] Liu, L., Qu, D., Cao, H., Huang, X., Song, Y., Kang, X. "Process optimization of high machining efficiency and low surface defects for HSD milling UD-CF/PEEK with limited thermal effect", *Journal of Manufacturing Processes*, 76, pp. 532–547, 2022. <https://doi.org/10.1016/j.jmapro.2022.02.040>
- [6] Gomez, M., Schmitz, T. "Stability Evaluation for a Damped, Constrained-motion Cutting Force Dynamometer", *Journal of Manufacturing and Materials Processing*, 6(1), 23, 2022. <https://doi.org/10.3390/jmmp6010023>
- [7] Schmitz, T. L., Smith, K. S. "Machining Dynamics: Frequency Response to Improved Productivity", Springer, 2009. ISBN 978-3-319-93706-9 <https://doi.org/10.1007/978-3-319-93707-6>
- The stiffness of the robot changes when the ductility and heterogeneity of the material are high; therefore, its effect was modeled by an auxiliary variable of qualitative nature.
- Dimensional quality during the robotic drilling process occurs when feed rate and rotation speed are low.
- Damage to the machined surface and degradation of dimensional quality occurs mainly at higher feed rates and cutting speeds. The effect of the latter reveals that the system takes vibrations that increase the cutting forces and disturb the drilling path.
- Finally, the improvement of the stability of the robot during the material removal can be considered by a thermal treatment able to bring better performances of the robot.

#### Acknowledgements

The authors would like to thank the Laboratory of Mechanics and Advanced Energy Systems (LMSEA), Laboratory of Structural Mechanics and Materials (LaMSM) and Directorate General for Scientific Research and Technological Development (DGRSDT) for funding this research study. In addition, the authors also highly appreciated the technical support of the University of Batna 2 and the National Polytechnic School of Constantine.

- [8] Altintas, Y. "Manufacturing automation: Metal cutting mechanics, machine tool vibrations, and CNC design", Cambridge University Press, 2000. ISBN 9780521659734
- [9] Narayanan, M. "Manufacturing processes", In: Webster, J. G. (ed.) Wiley Encyclopedia of Electrical and Electronics Engineering, John Wiley & Sons, 1999. ISBN 9780471346081  
<https://doi.org/10.1002/047134608X.W3810>
- [10] Thusty, J., Andrews, G. C. "A critical review of sensors for unmanned machining", *CIRP Annals*, 32(2), pp. 563–572, 1983.  
[https://doi.org/10.1016/S0007-8506\(07\)60184-X](https://doi.org/10.1016/S0007-8506(07)60184-X)
- [11] Byrne, G., Dornfeld, D., Denkena, B. "Advancing cutting technology", *CIRP Annals*, 52(2), pp. 483–507, 2003.  
[https://doi.org/10.1016/S0007-8506\(07\)60200-5](https://doi.org/10.1016/S0007-8506(07)60200-5)
- [12] Scippa, A., Sallese, L., Grossi, N., Campatelli, G. "Improved dynamic compensation for accurate cutting force measurements in milling applications", *Mechanical Systems and Signal Processing*, 54–55, pp. 314–324, 2015.  
<https://doi.org/10.1016/j.ymssp.2014.08.019>
- [13] Teti, R., Jemielniak, K., O'Donnell, G., Dornfeld, D. "Advanced monitoring of machining operations", *CIRP Annals*, 59(2), pp. 717–739, 2010.  
<https://doi.org/10.1016/j.cirp.2010.05.010>
- [14] Gautschi, G. "Piezoelectric Sensorics: Force, Strain, Pressure, Acceleration and Acoustic Emission Sensors, Materials and Amplifiers", *Sensor Review*, 22(4), pp. 363–364, 2002.  
<https://doi.org/10.1108/sr.2002.22.4.363.2>
- [15] Gautschi, G. H. "Cutting Forces in Machining and Their Routine Measurement with Multi-Component Piezo-Electric Force Transducers", In: Koenigsberger, F., Tobias, S. A. (eds.) *Proceedings of the Twelfth International Machine Tool Design and Research Conference*, Palgrave, 1972, pp. 113–120. ISBN 978-1-349-01399-9  
[https://doi.org/10.1007/978-1-349-01397-5\\_15](https://doi.org/10.1007/978-1-349-01397-5_15)
- [16] Iglesias, I., Sebastián, M. A., Ares, J. E. "Overview of the state of robotic machining: Current situation and future potential", *Procedia Engineering*, 132, pp. 911–917, 2015.  
<https://doi.org/10.1016/j.proeng.2015.12.577>
- [17] Kim, S. H., Nam, E., Ha, T. I., Hwang, S.-H., Lee, J. H., Park, S.-H., Min, B.-K. "Robotic Machining: A Review of Recent Progress", *International Journal of Precision Engineering and Manufacturing*, 20(9), pp. 1629–1642, 2019.  
<https://doi.org/10.1007/s12541-019-00187-w>
- [18] Verl, A., Valente, A., Melkote, S., Brecher, C., Ozturk, E., Tunc, L. T. "Robots in machining", *CIRP Annals*, 68(2), pp. 799–822, 2019.  
<https://doi.org/10.1016/j.cirp.2019.05.009>
- [19] Mousavi, S., Gagnol, V., Bouzgarrou, B. C., Ray, P. "Stability optimization in robotic milling through the control of functional redundancies", *Robotics and Computer-Integrated Manufacturing*, 50, pp. 181–192, 2018.  
<https://doi.org/10.1016/j.rcim.2017.09.004>
- [20] Dumas, C., Caro, S., Garnier, S., Furet, B. "Joint stiffness identification of six-revolute industrial serial robots", *Robotics and Computer-Integrated Manufacturing*, 27(4), pp. 881–888, 2011.  
<https://doi.org/10.1016/j.rcim.2011.02.003>
- [21] Caro, S., Dumas, C., Garnier, S., Furet, B. "Workpiece placement optimization for machining operations with a KUKA KR270-2 robot", In: 2013 IEEE International Conference on Robotics and Automation, Karlsruhe, Germany, 2013, pp. 2921–2926. ISBN 978-1-4673-5641-1  
<https://doi.org/10.1109/ICRA.2013.6630982>
- [22] Bauer, J., Friedmann, M., Hemker, T., Pischan, M., Reinl, C., Abele, E., von Stryk, O. "Analysis of industrial robot structure and milling process interaction for path manipulation", In: Denkena, B., Hollmann, F. (eds.) *Process Machine Interactions: Prediction and Manipulation of Interactions between Manufacturing Processes and Machine Tool Structures*, Springer, 2013, pp. 245–263. ISBN 978-3-642-32447-5  
[https://doi.org/10.1007/978-3-642-32448-2\\_11](https://doi.org/10.1007/978-3-642-32448-2_11)
- [23] Alici, G., Shirinzadeh, B. "Enhanced stiffness modeling, identification and characterization for robot manipulators", *IEEE Transactions on Robotics*, 21(4), pp. 554–564, 2005.  
<https://doi.org/10.1109/TRO.2004.842347>
- [24] Robin, V., Sabourin, L., Gogu, G. "Optimization of a robotized cell with redundant architecture", *Robotics and Computer-Integrated Manufacturing*, 27(1), pp. 13–21, 2011.  
<https://doi.org/10.1016/j.rcim.2010.06.010>
- [25] Pan, Z., Zhang, H., Zhu, Z., Wang, J. "Chatter analysis of robotic machining process", *Journal of Materials Processing Technology*, 173(3), pp. 301–309, 2006.  
<https://doi.org/10.1016/j.jmatprotec.2005.11.033>
- [26] Tunc, L. T., Shaw, J. "Investigation of the effects of Stewart platform-type industrial robot on stability of robotic milling", *The International Journal of Advanced Manufacturing Technology*, 87(1–4), pp. 189–199, 2016.  
<https://doi.org/10.1007/s00170-016-8420-z>
- [27] Wang, J., Zhang, J., Yao, Z., Yang, X., Sun, R., Zhao, Y. "Nonlinear characteristics of a multi-degree-of-freedom spur gear system with bending-torsional coupling vibration", *Mechanical Systems and Signal Processing*, 121, pp. 810–827, 2019.  
<https://doi.org/10.1016/j.ymssp.2018.12.002>
- [28] Henzold, G. "Geometrical dimensioning and tolerancing for design, manufacturing and inspection: A handbook for geometrical product specification using ISO and ASME standards", Butterworth-Heinemann, 2006. ISBN 978-0-7506-6738-8
- [29] Srinivasan, V. "Standardizing the specification, verification, and exchange of product geometry: Research, status and trends", *Computer-Aided Design*, 40(7), pp. 738–749, 2008.  
<https://doi.org/10.1016/j.cad.2007.06.006>
- [30] Derringer, G., Suich, R. "Simultaneous optimization of several response variables", *Journal of Quality Technology*, 12(4), pp. 214–219, 1980.  
<https://doi.org/10.1080/00224065.1980.11980968>